*Bull. Mater. Sci.*, Vol. 40, No. 7, December 2017, pp. 1291–1299
https://doi.org/10.1007/s12034-017-1498-6



# Synthesis, structure and thermoelectric properties of $La_{1-x}Na_xCoO_3$ perovskite oxides

**SUKANTI BEHERA[1], VINAYAK B KAMBLE[2,4], SATISH VITTA[3], ARUN M UMARJI[2,*] and C SHIVAKUMARA[1]**

[1]Solid State and Structural Chemistry Unit, Indian Institute of Science, Bengaluru 560012, India
[2]Materials Research Centre, Indian Institute of Science, Bengaluru 560012, India
[3]Department of Metallurgical Engineering and Materials Science, Indian Institute of Technology, Mumbai 400076, India
[4]School of Physics, Indian Institute of Science Education and Research, Thiruvananthapuram 695016, India
*Author for correspondence (umarji@mrc.iisc.ernet.in)

MS received 22 November 2016; accepted 24 March 2017; published online 7 December 2017

**Abstract.** Monovalent ion doped lanthanum cobaltate $La_{1-x}Na_xCoO_3$ ($0 \leq x \leq 0.25$) compositions were synthesized by the nitrate–citrate gel combustion method. All the heat treatments were limited to below 1123 K, in order to retain the Na stoichiometry. Structural parameters for all the compounds were confirmed by the Rietveld refinement method using powder X-ray diffraction (XRD) data and exhibit the rhombhohedral crystal structure with space group *R*-3*c* (No. 167). The scanning electron microscopy study reveals that the particles are spherical in shape and sizes, in the range of 0.2–0.5 μm. High temperature electrical resistivity, Seebeck coefficient and thermal conductivity measurements were performed on the high density hot pressed pellets in the temperature range of 300–800 K, which exhibit p-type conductivity of pristine and doped compositions. The X-ray photoelectron spectroscopy (XPS) studies confirm the monotonous increase in $Co^{4+}$ with doping concentration up to $x = 0.15$, which is correlated with the electrical resistivity and Seebeck coefficient values of the samples. The highest power factor of 10 μW $mK^{-2}$ is achieved for 10 at% Na content at 600 K. Thermoelectric figure of merit is estimated to be $\sim 1 \times 10^{-2}$ at 780 K for 15 at% Na-doped samples.

**Keywords.** Nitrate–citrate gel combustion method; perovskite; monovalent ions doping; semiconductor; thermoelectric.

## 1. Introduction

The energy requirements have increased manifold with time. Conventional energy has failed to meet requirements due to the increase in energy consumption. The aforementioned energy crisis has led the research in the direction of the alternative unconventional energy sources. In this scenario, phenomenon of thermoelectricity has been the hot topic of research in these days owing to its ability to convert waste thermal energy into an electrical energy [1]. The efficiency of a thermoelectric device is represented by figure of merit (zT), which is defined by equation (1) [2]

$$\text{Figure of merit (zT)} = \left(\frac{S^2\sigma T}{\kappa}\right), \tag{1}$$

where $S$ is the thermopower (also known as Seebeck coefficient); $\sigma$ is the electrical conductivity; $\kappa$ is the total thermal conductivity and $T$ is the absolute temperature. The materials such as intermetallic alloys, clatharates, chalcogenides, skutterudites, etc., have been the primary choice for thermoelectric applications. The oxides in the past were not considered as suitable materials for thermoelectric applications due to their low carrier mobility and strong ionic character between cation and anions. However, soon after the first report of thermoelectricity by Terasaki *et al* [3] on $NaCo_2O_4$ single crystal in 1997, there has been considerable recent interest in different oxides for the exploration of thermoelectric properties due to their observed reasonable figure of merit. Although $NaCo_2O_4$ is metallic, quite large thermopower (100 μV $K^{-1}$ at 300 K) is observed due to charge and different spins of cobalt ions. Most importantly, the oxides precede over the other class of materials due to their high thermal stability, non-toxicity and are known to be cost-effective as well as energy-efficient synthesis methods [4] though having a low thermoelectric figure of merit. The oxides, i.e., transition metal oxides are strongly correlated systems, where both the spin as well as the orbital degrees of freedom of charge carriers contribute towards the thermopower ($S$). Particularly, in case of cobaltate system, the spin states (i.e., low spin (LS), high spin (HS) and intermediate spin (IS)), play a crucial role in determining the thermopower ($S$), which is generally dependent on the temperature [5,6]. The temperature may trigger a transition in this system from LS to HS through an intermediate spin state, but still there is ambiguity regarding the different spin states with temperature. The cobaltate systems, viz., $Na_xCoO_2$, $Bi_2Sr_2Co_2O_x$ and $Ca_3Co_4O_9$ are layered structures consisting of alternate

stacking of electrically conducting $CoO_2$ layers and thermally insulating $Na^+$ and $MO_2$ layers, respectively [1,3,7].

The $ABO_3$ type perovskite oxides such as $La_{1-x}M_xCoO_3$ [8–14], $SrTiO_3$ [15], $CaMnO_3$ [15] have been reported to exhibit reasonable thermoelectric properties. The perovskite system is of crucial significance as the three interrelated terms, viz., Seebeck coefficient ($S$), electrical conductivity ($\sigma$) and thermal conductivity ($\kappa$) can be engineered by specific doping [16]. Various studies on bi-valent ions doping at A or B site in the $ABO_3$ perovskite have indicated the improvement in the zT as well as have led to the reduction in the lattice thermal conductivity by enhanced impurity scattering [9,12,14,17]. However, the effect of monovalent ions, Na doping on A-site has been rarely investigated in $LaCoO_3$ [18] due to volatile nature of monovalent ions at higher synthesis temperature. The monovalent ion doping at La site (A-site), leads to the formation of a hole, which is compensated by the oxidation of $Co^{3+}$ to $Co^{4+}$ ions in order to maintain the charge neutrality. Thus, the monovalent ion doping is expected to increase the carrier concentration, which may subsequently enhance the thermopower. Our approach is to find the effect of thermoelectric properties on the monovalent ion doping on A-site of $LaCoO_3$ system. Here, we report the synthesis of $Na^+$-ions doped $LaCoO_3$ samples by the nitrate–citrate gel combustion method at relatively low temperature (1123 K) and shorter duration (4 h). The structural, morphological and transport property measurements are carried out in order to evaluate thermoelectric parameters.

## 2. Experimental

$La_{1-x}Na_xCoO_3$ ($0 \leq x \leq 0.25$) compounds were synthesized by the nitrate–citrate gel combustion (NCG) method [16]. The NCG method is a solution-based method where the citrate gel ensures homogeneous distribution of cations. Upon low temperature pyrolysis due to autocombustion the product retains uniform cation distribution even at low concentrations. The redox reaction between the nitrate (oxidizer) and citrate gel (fuel) sets in after all the volatile components evaporate, thus the role of pH is negligible. High purity starting materials of $La_2O_3$ (preheated at 800°C for 3 h), $Na_2CO_3$, $CoC_2O_4{\cdot}2H_2O$ and citric acid were used. The typical preparation of $La_{0.9}Na_{0.1}CoO_3$ compound was included in the following steps: stoichiometric amounts of $La_2O_3$, $Na_2CO_3$ and $CoC_2O_4{\cdot}2H_2O$ were dissolved in 20 ml of 8 N $HNO_3$ to get metal nitrate solution. Separately, citric acid (1:3 molar ratio) was dissolved in 50 ml of distilled water and added to the metal ions containing nitrate solution. The pink colour solution was heated on a hot plate around 373 K to remove the water for obtaining a thick viscous gel, which heated further to 643 K yielded black powder. Finally, the powder was transferred into a porcelain crucible and calcined at 1123 K for 4 h in a muffle furnace to form crystalline compounds.

The phase purity of compounds were studied by the powder X-ray diffraction (XRD) on PANalytical X-pert Pro instrument with Cu kα radiation ($\lambda = 1.5418$ Å) using a nickel filter. For Rietveld refinement analysis, data were collected at a scan rate of 2° $min^{-1}$ with a 0.033° step size for $2\theta$ ranging from 10 to 82°. The structural parameters were refined by Rietveld method using FullProf Suite-2000 software. The morphology and elemental mapping of samples were examined using Carl Zeiss scanning electron microscope (SEM) coupled with EDS. The crystallinity and sizes were further confirmed by using FEI TECNAI F30 S-TWIN transmission electron microscope (TEM). The elemental compositions and the oxidation states were evaluated using AXIS ULTRA X-ray photoelectron spectroscopy (XPS) of Al $K_\alpha$ (1486.5 eV) incident photon energy. The binding energy correction is done using C1s of graphite at 284.5 eV as reference and reported with an accuracy of ±0.5 eV. The powder samples were made into pellets of diameter $\varphi \sim 12.7$ mm using uniaxial hot pressing by applying 29 MPa for 5 min at 973 K. The pellets were further annealed at the same temperature (973 K) for 6 h in ambient atmosphere. The densities of all compositions were in the range of 70–75% as measured by Archimedes method using isopropyl alcohol solvent. The samples are coded and summarized in table 1. The Seebeck coefficient and the electrical resistivity measurements were performed on annealed pellets by using ULVAC ZEM-3 (Japan) in the temperature range of 300–800 K. Bar shaped samples ($2 \times 2 \times 10$ mm) are clamped between hot and cold blocks of the sample holder. Two S-type sensing thermocouples are in pressure contact at a distance of 6 mm. For Seebeck measurement, after equilibrating the hot block temperature the temperature difference ($\Delta T$) is measured by the two thermocouples in a differential way and the Seebeck voltage ($\Delta V$) is measured by the Pt lead of the same thermocouple. For four probe resistance measurements, the measuring current is passed through the clamping blocks and the voltage drop is measured by the Pt leads of the sensing thermocouples.

Thermal diffusivity measurement of 12.7 mm diameter and 2-mm thick samples were performed on Netzsch laser flash instrument, specific heat by DSC and density measured by bulk sample and/or Archimedes principle and thermal conductivity is then calculated using the equation (2).

**Table 1.** Nominal compositions with respective codes for sodium-doped $LaCoO_3$ perovskite oxides.

| Compositions | Code |
|---|---|
| $LaCoO_3$ | LCO |
| $La_{0.95}Na_{0.05}CoO_3$ | LNCO5 |
| $La_{0.90}Na_{0.10}CoO_3$ | LNCO10 |
| $La_{0.85}Na_{0.15}CoO_3$ | LNCO15 |
| $La_{0.80}Na_{0.20}CoO_3$ | LNCO20 |
| $La_{0.75}Na_{0.25}CoO_3$ | LNCO25 |

$$\kappa = \alpha C_p d, \tag{2}$$

where $\alpha$ is the thermal diffusivity, $C_p$ = specific heat and $d$ is density of the sample.

## 3. Results and discussion

### 3.1 *X-ray diffraction*

Figure 1 shows the powder X-ray diffraction patterns of sodium-doped lanthanum cobaltate (LNCO) composition.

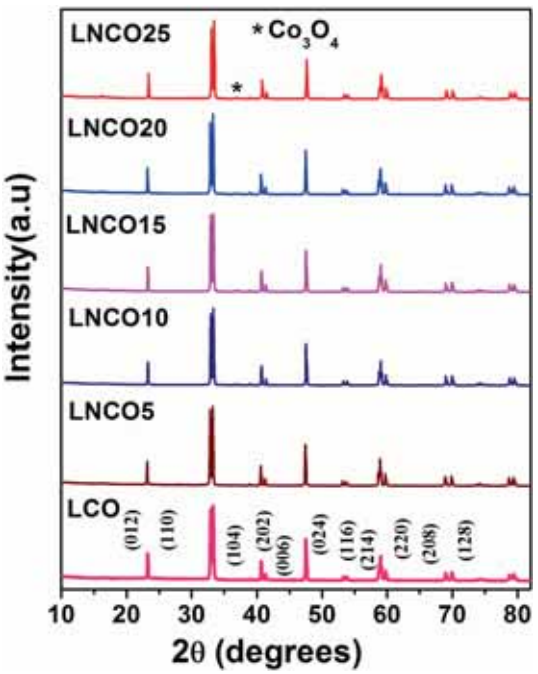


**Figure 1.** Powder XRD patterns of Na-doped $LaCoO_3$ compounds.

All the compositions were indexed to the rhombohedral structure with a hexagonal setting of the standard JCPDS card No. 86-1663. When doping content $\geq$ 0.20, there is a small amount ($\sim$3%) of an impurity ($Co_3O_4$) phase observed. Hence, for property evaluation only monophasic compositions (i.e., $x = 0.15$) were considered. Structural parameters for all compositions were refined by the Rietveld refinement method using FullProf Suite software package. The patterns were typically refined for lattice parameters, scale factor, backgrounds, pseudo-Voigt profile function (u, v and w), atomic coordinates and overall isothermal temperature factors ($B_{iso}$). Figure 2 shows the observed, calculated and the difference in XRD patterns typically for (a) LNCO5 and (b) LNCO15. There is a good fitting between the observed and calculated patterns. The refinement results are in agreement with JCPDS database that all the compositions crystallize in the rhombhohedral structure (hexagonal setting) with space group $R\bar{3}c$ (No. 167). On substitution of monovalent sodium ions to $La^{3+}$-site in the LCO compound, no structural transition was observed. The ionic radii of the cations are $r_{La^{3+}} = 1.36$ Å; $r_{Na^{+}} = 1.39$ Å for 12-fold coordination. The lattice parameters and cell volume did not show any significant change. This change due to substitution of $Na^{+}$ on $La^{3+}$-site resulting in $Co^{3+}$ getting oxidized to $Co^{4+}$, which has smaller ionic radii ($r_{Co^{4+}} = 0.53$ Å compared to $r_{Co^{3+}} = 0.61$ Å) that compensates the overall cell volume value. The crystal structure of all the compositions were modelled through VESTA program using the Rietveld refined structural parameters and the typical crystal structure of $La_{0.85}Na_{0.15}CoO_3$ sample is shown in figure 3. Figure 4 shows the typical XRD patterns for LNCO5 compound, (i) calcined powder at 1123 K, (ii) powder obtained from the hot pressed pellet and (iii) hot pressed pellet followed by annealing at 973 K in ambient atmosphere. From figure 4a–c it is confirmed that there is no structural change in both the hot pressed and hot pressed annealed samples.

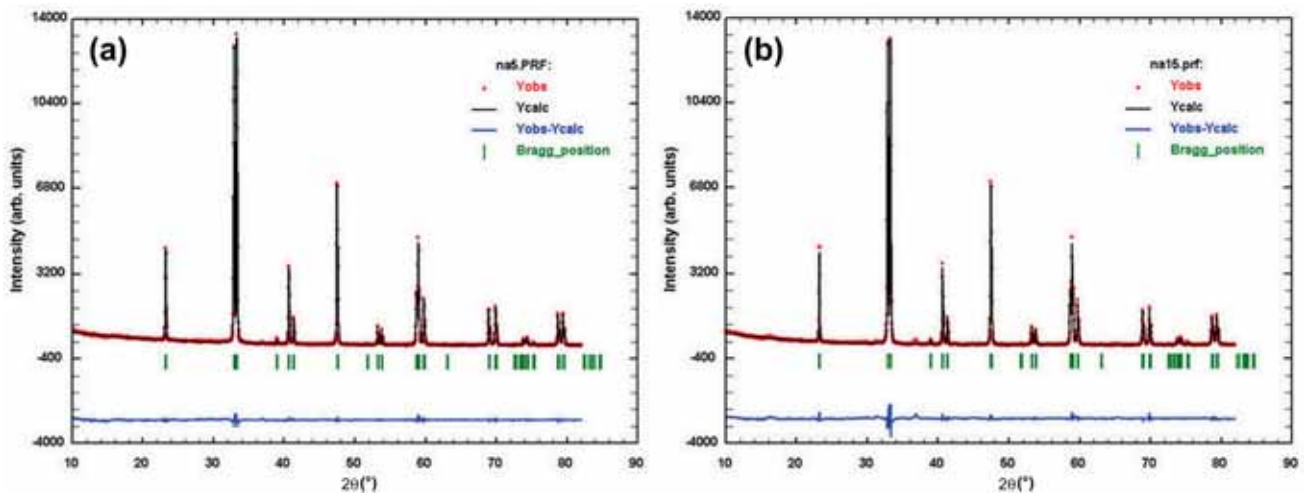


**Figure 2.** Observed, calculated and the different XRD patterns for (**a**) LNCO5 and (**b**) LNCO15.

### 3.2 *Scanning electron microscopy*

The average particle size of the pristine composition is ~0.3 microns. Figure 5 shows the SEM micrographs of (a) LNCO5 and (b) LNCO10 samples. The inset shows higher magnification SEM micrographs of respective compositions depicting individual particles. It is seen that the particle size increases with the dopant concentration and reaches to 0.2–0.5 μm. This may be attributed to liquid phase sintering of Na doping on $LaCoO_3$. Figure 6 shows the elemental mapping of a typically LNCO15 composition, which exhibits the homogeneous mixture of all La, Na and Co elements in the sample.

### 3.3 *Transmission electron microscopy*

Furthermore, the crystal structure and crystallite size of the compounds were confirmed by using the TEM study. Figure 7a shows a TEM image of LCO, where the crystallite size ~0.3 μm is estimated for the particles. The inset shows the selected area electron diffraction (SAED) pattern, which is indexed as (012), (024) and (110) reflections. The high-resolution transmission electron microscopy (HRTEM) (shown in figure 7b), reveals a d-spacing of 0.38 nm, which corresponds to (012) reflection of $LaCoO_3$ perovskite structure. Similarly, the SAED pattern and HRTEM images of LNCO10 are shown in figure 7c and d, respectively. The HRTEM of LNCO10 also confirms the similar lattice spacing (0.375 nm) and particle size (shown inset in figure 7c) with SAED pattern indexed for (012) reflections and subsequent reflections as that of undoped LCO compound. The TEM results are in agreement with that of XRD studies.

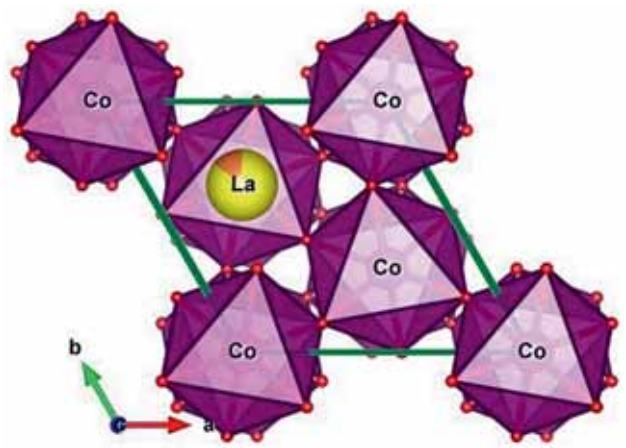


**Figure 3.** Crystal structure of $La_{1-x}Na_xCoO_3$.

### 3.4 *X-ray photoelectron spectroscopy*

On substitution of monovalent Na-ions to $La^{3+}$-site in $LaCoO_3$ system, $Co^{3+}$ ion gets oxidized to $Co^{4+}$ state, which

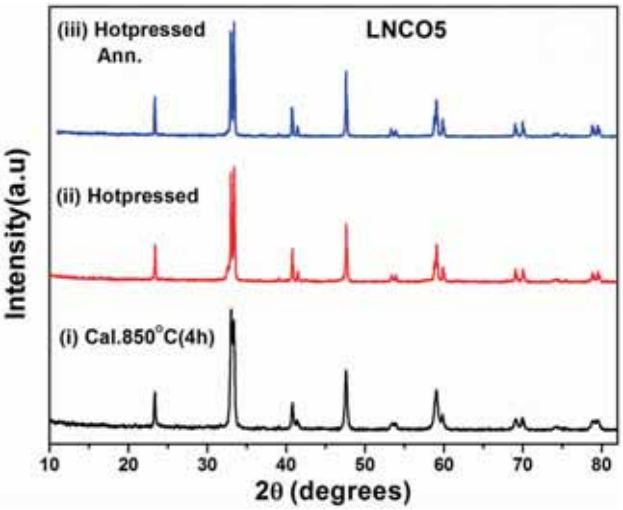


**Figure 4.** Powder XRD patterns of LNCO5 compound (i) calcinationed powder at 1123 K, (ii) powder obtained from the hot pressed pellet and (iii) annealed samples at 973 K.

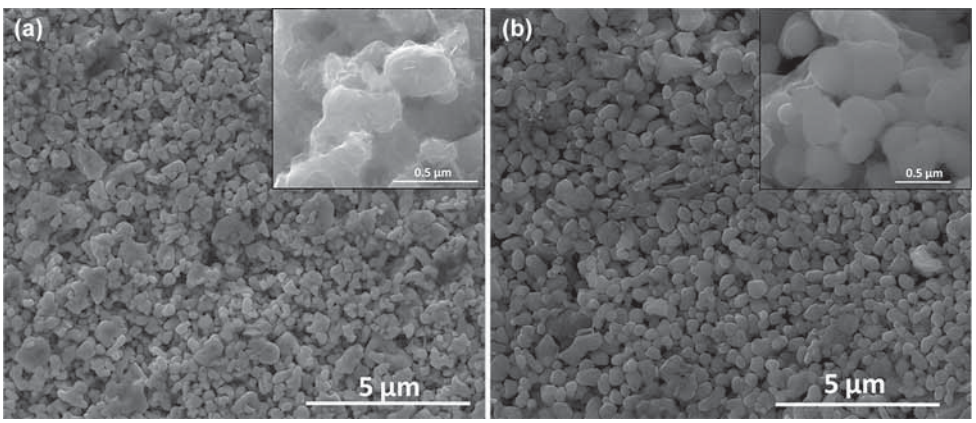


**Figure 5.** SEM images of (**a**) LNCO5 and (**b**) LNCO10 compositions.

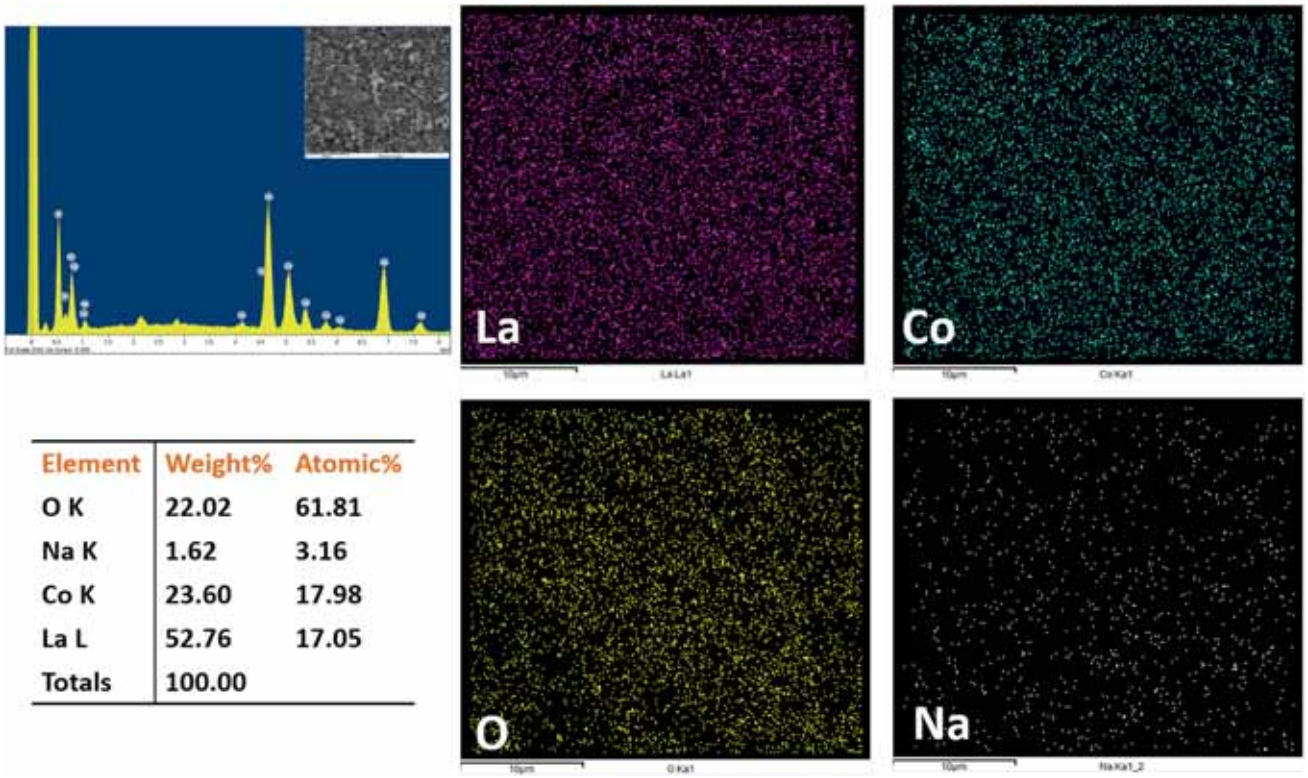


**Figure 6.** Elemental mapping of LNCO15 compositions.

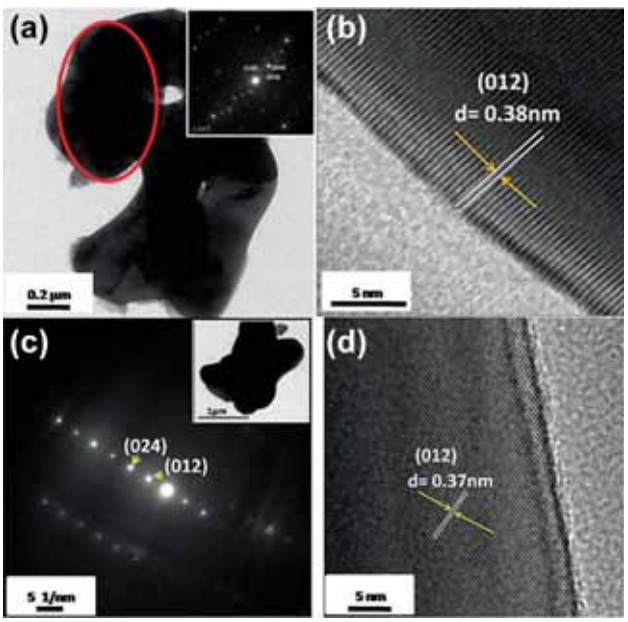


**Figure 7.** (**a**) TEM images of LCO, inset shows SAED pattern, (**b**) HRTEM image of LCO, (**c**) SAED pattern of LNCO10 and (**d**) HRTEM image of LNCO10.

was confirmed by the XPS study [19,20]. Figure 8 shows the XPS spectra of (a) La3d, (b) O1s, (c) Na1s and (d) Co 2p region of LNCO5 sample. La $3d_{3/2}$ and $3d_{5/2}$ peaks are observed around 854.4 and 833.8 eV, respectively, confirming $La^{3+}$ oxidation state. In addition, peaks at 837.5 and 850.8 eV are seen due to charge transfer from the neighbouring La atoms to the empty *4f* subshell in the ionization process, as reported in the literature [10]. The O 1s peaks at 528.6 eV shows an asymmetry due to lattice oxygen species ($O_{latt}$ : $O^{2-}$) and a shoulder peak at 531.2 eV due to adsorbed oxygen species ($O_2^{-2}$, $O^-$). In $LaCoO_3$, the semiconducting nature arises due to various oxidation states of cobalt ions. The Co peaks are deconvoluted to $Co^{3+}$ and $Co^{4+}$ main peaks along with certain known satellite peaks. It can be seen that as the Na content in the lattice increases, the concentration of $Co^{4+}$ also increases to compensate the charge neutrality of the system, which is accompanied by an increase in the hole concentration.

### 3.5 *Electrical resistivity*

The band gap of the pristine sample is found to be 0.12 eV, which decreases to 0.1 eV with increasing Na contents at La-site. Figure 9a shows the temperature dependence of resistivity of all the compositions in the temperature range of 300–800 K. The resistivity of pristine sample (LCO) is found to be 16 Ω cm at 316 K, which further decreases with the increasing temperature, demonstrating a semiconductor behaviour for pristine as well as doped samples. The values of resistivity obtained agree well with the reported work by

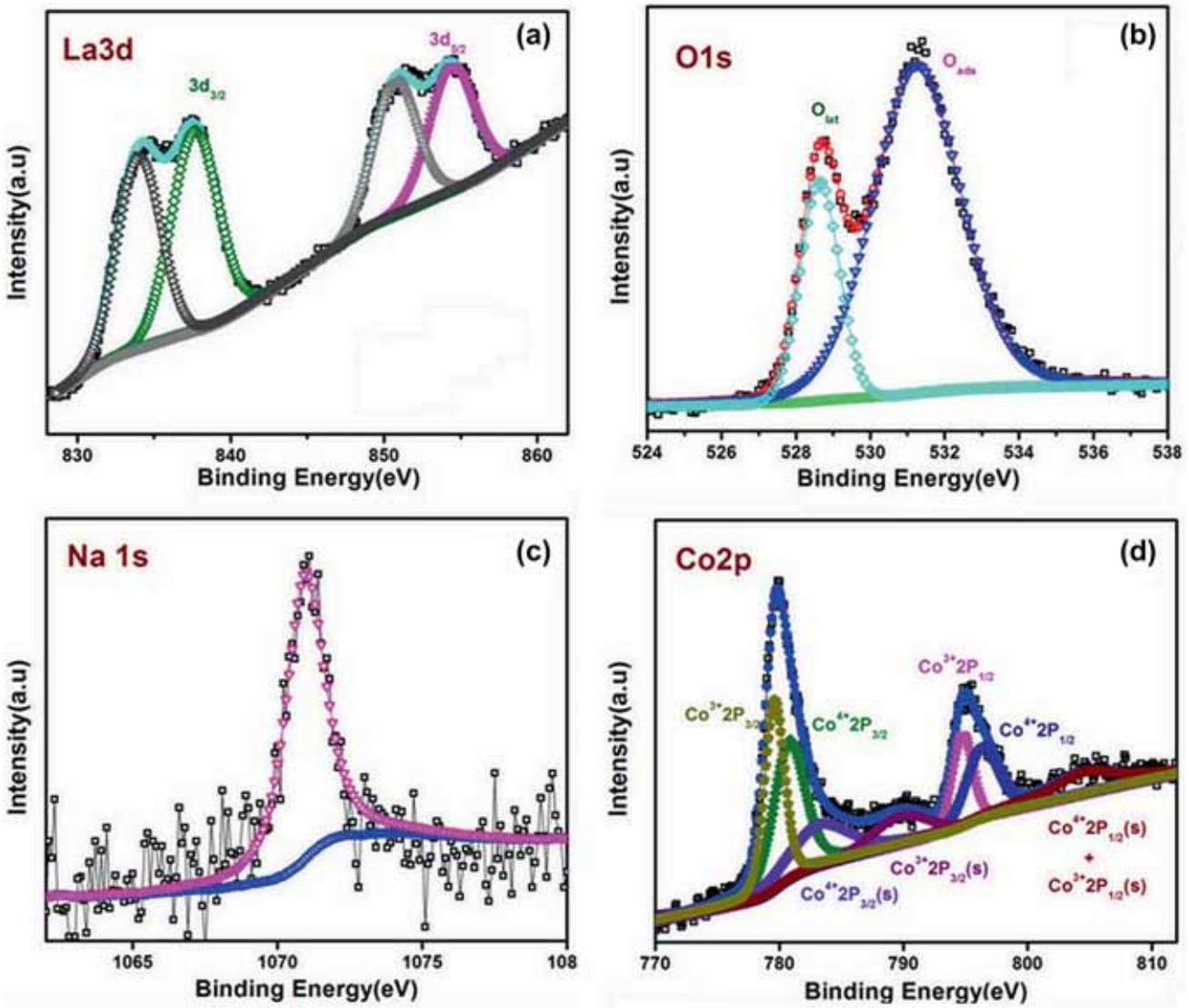


**Figure 8.** XPS spectrum of LNCO5 with enlarged region of (**a**) La3d, (**b**) O1s, (**c**) Na1s and (**d**) Co2p core level spectra of LNCO5.

He *et al* [18] for $La_{1-x}Na_xCoO_3$. It is observed that as the Na content increases, the resistivity decreases monotonously up to 10 at% Na doping (LNCO10), beyond which, it increases again. This increase in the electrical resistivity could be attributed to the saturation of carrier concentration or the presence of secondary phase of $Co_3O_4$ spinel structure in the LNCO15 composition. Although the secondary phase of $Co_3O_4$ could not be found within the resolution limit of XRD. At high temperatures ($T > 450$ K) lowering of electrical resistivity is observed. This dip in the onset of semiconductor to metal transition was observed elsewhere [21]. Thus, progressively doping at the La site is compensated by an increase in the Co ion non-stoichiometry from $Co^{3+}$ to $Co^{4+}$ ions, as also confirmed by the XPS studies. Mineshige *et al* [22] reported that when the temperature varies, Sr content's partial pressure affects the non-stoichiometry of Co and O on Sr-doped LCO. Similarly, in this study the doping of Na on La site creates excessive negative charge in the lattice and to maintain the charge neutrality holes are created such that $Co^{3+}$ is oxidized to $Co^{4+}$ ions as temperature and pressure were kept the same for all compositions.

### 3.6 *Seebeck coefficient*

Cobalt oxide systems are strongly correlated systems in which $S$ predominantly depends on the configurational entropy, concentration of $Co^{3+}$ and $Co^{4+}$ ions. The $La_{1-x}Sr_xCoO_3$ has shown large thermopower due to the strong electron correlations alongwith degeneracy of 3*d* orbitals of cobalt [23]. Figure 9b shows the effect of Na on temperature dependence of Seebeck coefficient ($S$). The parent samples show a larger

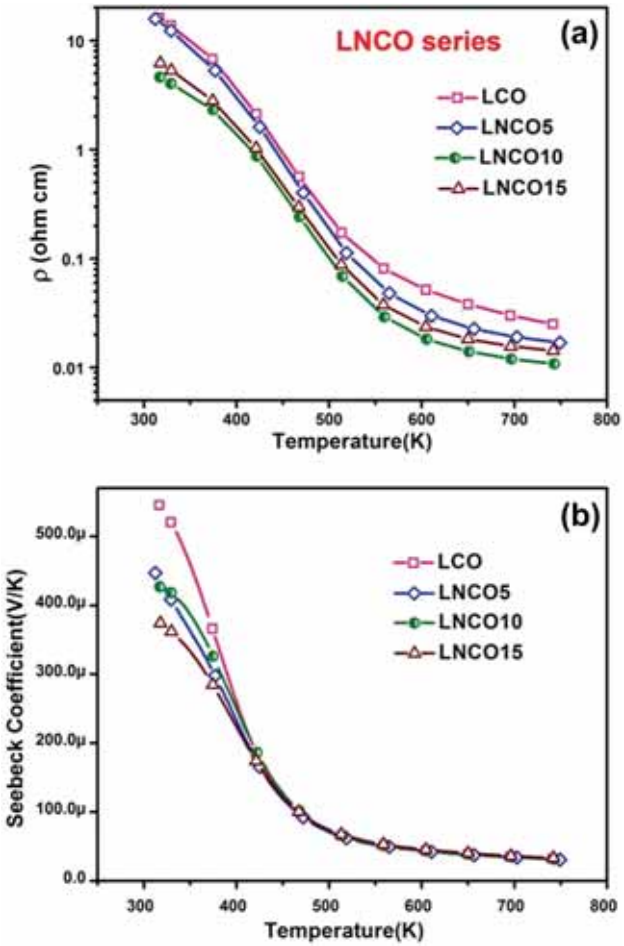


**Figure 9.** Temperature dependent study of (**a**) plots of electrical resistivity and (**b**) Seebeck coefficient of $La_{1-x}Na_xCoO_3$ compositions.

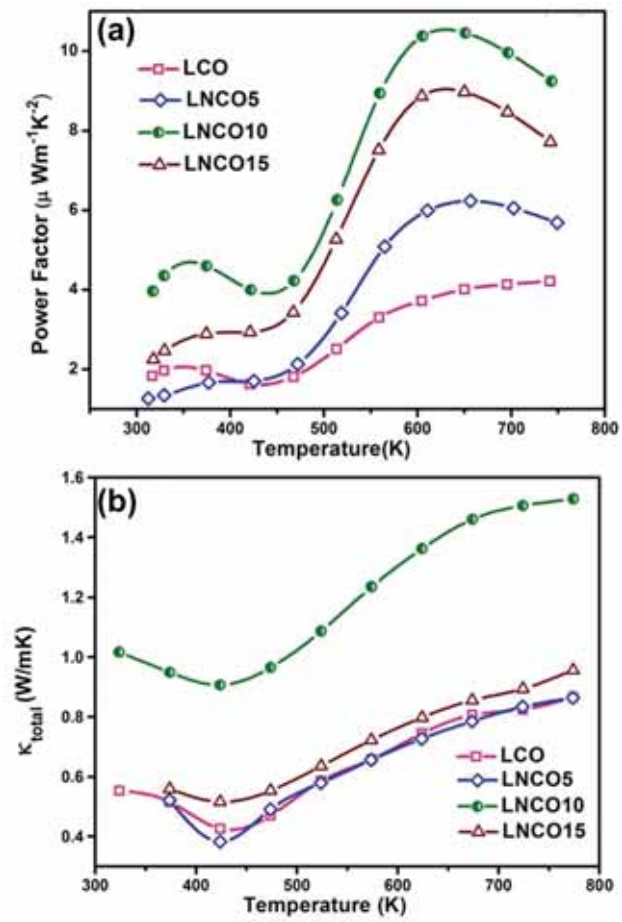


**Figure 10.** (**a**) Power factor and (**b**) the total thermal conductivity LNCO.

positive Seebeck coefficient value of 545 μV $K^{-1}$ than doped samples at 318 K. Although both positive and negative values of Seebeck coefficients have been reported in the literature for LCO [24,25]; recently, Herbert *et al* [26] found that a small change in the hole by $Sr^{2+}$ or electron concentration by $Ce^{4+}$ and $Ti^{4+}$ alter the parity of $S$ from positive to negative value.

It is seen that at room temperatures, the $S$-value decreases monotonously with doping of sodium $La_{1-x}Na_xCoO_3$ from 545 to 374 μV $K^{-1}$. This monotonous decrease in $S$-value with increasing Na content is attributed to the increase in the hole concentration ($n$). As temperature increases, difference in the value of $S$ for doped and the pristine sample decreases. Owing to the thermal activation of holes in the pristine sample and as further temperature increases, difference in the carrier concentration of doped and undoped sample decreases as described by Iwasaki *et al* [9]. Hence, at higher temperature $S$-values are independent of doping. In this temperature range, the thermopower is known to obey generalized Heike's formula. The $S$-values are found to be governed by chemistry rather than the carrier concentration. According to generalized Heike's formula [23,27].

$$S = -\frac{k_\beta}{e} \ln \frac{g_3}{g_4} \frac{x}{1-x},$$

where $k_\beta$ = Boltzmann's constant, $e$ = electronic charge, $g_3$, $g_4$ = number of possible configuration of $Co^{3+}$, $Co^{4+}$ ions, respectively, and $x$ = concentration of $Co^{4+}$ ions. The thermopower ($S$) from the above equation indicates that it is dependent on both the ratio of $g_3/g_4$ and configuration of $Co^{3+}$, $Co^{4+}$ ions. In addition, the conduction occurs due to the hole hopping between [$Co^{3+}$] and [$Co^{4+}$], which is independent of temperature.

Using the properties measured, power factor ($S^2\sigma$) is calculated and the maximum power factors are obtained, i.e., 10 μW m$K^{-2}$ of LNCO15 at 600 K as shown in figure 10a, corresponds to optimized electrical conductivity and thermopower. For all the compositions, $La_{1-x}M_xCoO_3$, $S$-values are found to decrease with the increasing dopant concentration, however, at higher temperatures (typically >450 K) the Seebeck value becomes independent of doping concentration. In the $S$ *vs.* $T$ curve a sharp dip is also observed at ~450 K due to $I-M$ transition as discussed earlier in the resistivity as a function of temperature curve.

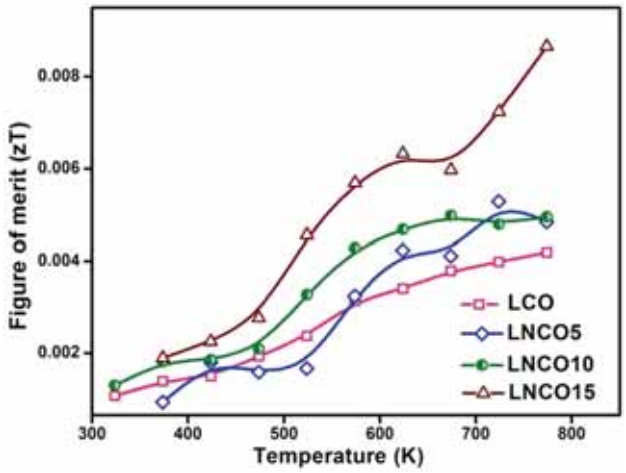


**Figure 11.** Figure of merit (zT) of LNCO compositions.

### 3.7 *Thermal conductivity*

Oxides are known for lower thermal conductivity. Figure 10b depicts the variation of the total thermal conductivity ($\kappa_{\text{total}}$) of Na-doped samples, respectively, in the temperature range 300–800 K. The parent $LaCoO_3$ is semiconducting in nature, the lattice thermal conductivity ($\kappa_l$) plays a dominant role and is estimated by subtracting the electronic part of thermal conductivity ($\kappa_e$) from total thermal conductivity ($\kappa_{\text{total}}$). Here, the $\kappa_e$ is evaluated using Wiedemann–Franz law as shown in equation (2).

$$\kappa_e = L_0 \sigma T, \tag{3}$$

where $L_0$ is the Lorentz number $2.45 \times 10^{-8}$ W$\Omega$ K$^{-2}$, $\sigma$ is electrical conductivity and $T$ is the absolute temperature. The LNCO10 composition shows the highest thermal conductivity of 1.01 W mK$^{-1}$ at 323 K compared to all the other Na-doped samples. This maxima may be a result from the higher electrical conductivity and hence, leads to the higher total thermal conductivity $\kappa_{\text{total}}$ ($\kappa_{\text{total}} = \kappa_e + \kappa_{\text{lat}}$). The thermal conductivity is found to increase with increasing temperature for all the compositions [28]. The thermal conductivity of 1.5 W mK$^{-1}$ is at 750 K for LNCO10 compositions.

### 3.8 *Figure of merit*

The variation of thermoelectric zT of LNCO samples are depicted in figure 11. The zT lies between $1 \times 10^{-3}$ and $2 \times 10^{-3}$ at 325 K, which increases with increasing temperature. Although LNCO15 sample shows highest resistivity and a low Seebeck coefficient value than LNCO10, it is found to exhibit highest figure of merit, i.e., $9 \times 10^{-3}$ at 780 K.

## 4. Conclusions

The polycrystalline Na ions doped $LaCoO_3$ compounds were synthesized by the nitrate–citrate gel combustion method at relatively low temperature and shorter heat treatment duration. Powder XRD confirms the compositions are in single phase up to $x = 0.15$. The parent $LaCoO_3$ and doped compounds exhibit a semiconducting nature and the resistivity ($\rho$) is found to be in the range of 10–0.01 ohm cm for the hot pressed pellets. The parent compound shows high S value 545 $\mu$V K$^{-1}$ at 318 K, whereas for the highest doping concentrations of Na samples shows Seebeck values of $\sim$374 $\mu$V K$^{-1}$. The highest value of zT $\sim$0.01 is achieved in the $La_{0.85}Na_{0.15}CoO_3$ compound.

## Acknowledgements

We are thankful to Ms Kalpana Rajput for her operational help in using the thermal diffusivity instrument.

## References

[1] Mahan G, Sales B and Sharp J 1997 *Phys. Today* **42** 42
[2] Rowe D M 1995 *CRC handbook of thermoelectrics* (USA: CRC Press)
[3] Terasaki I, Sasago Y and Uchinokura K 1997 *Phys. Rev. B* **56** R12685
[4] He Yufei J L, Funahashi and Ryoji 2011 *J. Mater. Res.* **26** 1762
[5] Raccah P M and Goodenough J B 1967 *Phys. Rev.* **155** 932
[6] Yamaguchi S, Okimoto Y, Taniguchi H and Tokura Y 1996 *Phys. Rev. B* **53** R2926
[7] Tritt T M and Subramanian M A 2006 *MRS Bull.* **31** 188
[8] Señarís-Rodríguez M A and Goodenough J B 1995 *J. Solid State Chem.* **116** 224
[9] Iwasaki K, Ito T, Nagasaki T, Arita Y, Yoshino M and Matsui T 2008 *J. Solid State Chem.* **181** 3145
[10] Jørgensen C K and Berthou H 1972 *Chem. Phys. Lett.* **13** 186
[11] Kun R, Populoh S, Karvonen L, Gumbert J, Weidenkaff A and Bbusse M 2013 *J. Alloys Compd.* **579** 147
[12] Li F and Li J F 2011 *Ceram. Int.* **37** 105
[13] Robert R, Bocher L, Trottmann M, Reller A and Weidenkaff A 2006 *J. Solid State Chem.* **179** 3893
[14] Vulchev V, Vassilev L, Harizanova S, Khristov M, Zhecheva E and Stoyanova R 2012 *J. Phys. Chem. C* **116** 13507
[15] Sootsman J R, Chung D Y and Kanatzidis M G 2009 *Angew. Chem. Int. Edt.* **48** 8616
[16] Sndroulakis J, Migiakis P and Giapintzakis J 2004 *Appl. Phys. Lett.* **84** 1099
[17] Durá O J, Rogl P, Falmbigl M, Hilscher G and Bauer E 2012 *J. Appl. Phys.* **111** 063722
[18] He T, Chen J, Calvarese T G and Subramanian M A 2006 *Solid State Sci.* **8** 467
[19] Dupin J C, Gonbeau D, Benqlilou-Moudden H, Vinatier P and Levasseur A 2001 *Thin Solid Films* **384** 23
[20] Meza E, Ortiz J, Ruíz-León D, Marco J F and Gautier J L 2012 *Mater. Lett.* **70** 189

[21] Knížek K, Jirák Z, Hejtmánek J, Veverka M, Maryško M, Maris G *et al* 2005 *Euro. Phys. J. B* **47** 213
[22] Mineshige A, Kobune M, Fujii S, Ogumi Z, Inaba M, Yao T *et al* 1999 *J. Solid State Chem.* **142** 374
[23] Koshibae W, Tsutsui K and Maekawa S 2000 *Phys. Rev. B* **62** 6869
[24] Ohtani K K T, Matsugami K and Katoh D 2000 *J. Euro. Ceram. Soc.* **20** 2721
[25] Berggold M K K, Zobel C, Reichi A, Reuther M, Muller R, Freimuth A *et al* 2005 *Phys. Rev. B* **72** 155116
[26] Hébert S, Flahaut D, Martin C, Lemonnier S, Noudem J, Goupil C *et al* 2007 *Prog. Solid State Chem.* **35** 457
[27] Chaikin P M and Beni G 1976 *Phys. Rev. B* **13** 647
[28] Robert R, Aguirre M H, Hug P, Reller A and Weidenkaff A 2007 *Acta Mater.* **55** 4965